ADVANCED FUNCTIONAL MATERIALS
www.afm-journal.de

Materials Views
www.MaterialsViews.com

Modification of PCBM Crystallization via Incorporation of C_{60} in Polymer/Fullerene Solar Cells

*Jeffrey J. Richards, Andrew H. Rice, Rainie D. Nelson, Felix S. Kim, Samson A. Jenekhe, Christine K. Luscombe, and Danilo C. Pozzo**

The morphological effects of the incorporation of C_{60} into blended thin-films of poly(3-hexylthiophene) and [6,6]-phenyl C_{61} butyric acid methyl ester (PCBM) are investigated. The results show that addition of C_{60} readily alters the growth-rate and morphology of PCBM crystallites under different environmental conditions. The effect of C_{60} on the growth of large PCBM crystallites is thoroughly characterized using optical microscopy, electron microscopy and UV-visible absorption spectroscopy. Results show that C_{60} incorporation modifies fullerene aggregation and crystallization and greatly reduces the average crystallite size at C_{60} loadings of ≈50 wt% in the fullerene phase. Organic field-effect transistors (OFETs) are prepared to evaluate the electron mobility of PCBM/C_{60} films and organic solar cells (OSCs) are fabricated from mixed-fullerene active layers to evaluate their performance. It is demonstrated that the use of fullerene mixtures in organic electronic applications is a viable approach to produce more stable devices and to control the growth of micrometer-sized fullerene crystals.

1. Introduction

The morphology of small molecule, polymer, and protein crystals depends on super-saturation conditions, nucleation and growth kinetics, and on the termination mechanism of growing crystallites.[1] In many cases, it is desirable to form large, faceted crystals in order to obtain structural information using techniques such as X-ray diffraction. While there are many factors that influence the structure, size and quality of a crystal, one key factor to obtaining large crystallites is the purity of the components.[2] Impurities interfere with crystal growth and can also drive amorphous aggregation reducing crystal quality and preventing characterization via diffraction. In some cases, this effect is exploited to modify the natural habit of a crystal.[3] Examples of how such impurities affect crystal growth include adsorption to high energy crystal planes, lattice intercalation, seeding the formation of new nuclei, and capping crystal size (e.g., inorganic semiconductor quantum dots).[4]

In the production of organic solar cell (OSC) active layers, highly purified conjugated polymers and fullerene derivatives are often employed. The tendency of these materials to crystallize is viewed as critical to achieving the desired bulk-heterojunction morphology, an extended polymer/fullerene network with mesoscopic phase segregation.[5–7] The most common n-type semiconductor material used in OSCs, [6,6]-phenyl C_{61} butyric acid methyl ester (PCBM), frequently forms needle-like crystallites that have lengths and widths of tens of micrometers in dimension. These crystals tend to grow and develop inside polymer/fullerene thin-films, which are usually less than 1 μm thick, to form micrometer-sized crystals when they are annealed for extended periods of time or at very high temperatures.[8–10] It is now established that these "overgrown" PCBM crystallites represent an important degradation pathway that significantly affects the long-term performance of polymer/fullerene solar cells.[11,12] Conversely, the crystallization of the polymer phase in polymer/fullerene solar cells is usually beneficial. When some conjugated polymers crystallize, they form long fibers with nanometer cross-sectional dimensions.[13] For these polymers, such as poly(3-hexylthiophene) (P3HT) and poly(3-butylthiophene) (P3BT), the crystalline phase can have a significantly higher charge carrier mobility than the amorphous phase. Furthermore, the dimensions of the fibrillar aggregates are also of the order of the exciton diffusion distance so that charges can be effectively dissociated at the p/n material interface.[14–18] Crystallization of such conjugated polymers, therefore, facilitates the development of a bulk-heterojunction because pure polymer/fullerene blends spontaneously phase segregate during annealing leading to improved device performance.[19]

Crystallization for both the polymer and fullerene components in the solid state occurs at temperatures below their common miscibility point (T_{misc} = 205–290 °C for P3HT and PCBM depending on film composition) and above the glass transition of the polymer phase (T_{glass} = 12 °C).[20,21] There are no evident thermodynamic phase transitions in P3HT/PCBM blends between these two temperatures.[21] Phase segregation

J. J. Richards, R. D. Nelson, F. S. Kim,
Prof. S. A. Jenekhe, Prof. D. C. Pozzo
Department of Chemical Engineering
University of Washington
Seattle, WA 98195, USA
E-mail: dpozzo@u.washington.edu
A. H. Rice, Prof. C. K. Luscombe
Department of Material Science and Engineering
University of Washington
Seattle, WA 98195, USA

DOI: 10.1002/adfm.201201100

is therefore a thermodynamically driven process that will likely occur at any point within this temperature region. Nevertheless, the kinetics of the crystallization process will vary significantly with factors such as the environmental temperature, the concentration of dissolved PCBM, the viscosity of the polymer matrix and even the film thickness. Therefore, because of the simultaneous crystallization process, regardless of the specific thermal treatment, the instantaneous morphology that leads to a particular device performance is only a transient one and will likely continue to evolve with time even when the temperature is lowered. While quenching a film from the annealing temperature to ambient conditions slows the evolution of the film morphology, the polymer/fullerene films are still inherently unstable due to the finite solubility and relatively high mobility of PCBM in the amorphous conjugated polymer domains.[22,23] Films will continue to slowly evolve over time as the crystallization of both components proceeds. Under typical annealing conditions (120 °C < T_{anneal} < 170 °C), this effect manifests itself as a drop in solar cell performance when longer annealing times are used and PCBM crystal domains overgrow. Performance decreases once the crystal size exceeds the optimal size for ideal bulk heterojunctions because the total interface between p-type and n-type domains decreases with increasing domain size. However, even at modest operating temperatures for polymer solar cells (20 °C < T_{op} < 80 °C), slow structural evolution and performance degradation persists as a result of PCBM crystal growth.[24,25] This concept is shown schematically in **Figure 1**. This mechanism of degradation is not only a practical challenge for the optimization of active layer morphology in polymer solar cells, but also for making devices that have adequate lifetimes (years) at normal operating conditions.

There is a need to improve the thermal stability of polymer/fullerene solar cells by controlling the crystallization of the fullerene phase. Several strategies are currently being pursued. The first approach is the synthesis of compatibilizing agents that function to stabilize the polymer/fullerene interface.[26,27] For example Tsai et al. synthesized a poly(4-vinyltriphenylamine)/P3HT copolymer using quasi-living Grignard metathesis and living anionic polymerization.[28] These molecules have the potential to improve long-term thermal stability as they function like surfactants that prevent further coarsening of the polymer and fullerene phases, but more study is needed to understand the specific effects these materials have on the morphology of the active layers. A second approach that has been employed is the synthesis of fullerenes with different substitution moieties. Using novel chemical routes, it is possible to synthesize fullerenes that are not capable of packing into uniform crystals; therefore phase segregation is only driven by the crystallization of the polymer phase. This approach has been recently demonstrated with a new PCBM derivative consisting of 1,2-dihydromethano-[60] PCBM by Li et al.[29,30] This approach is highly desirable for conjugated polymers that crystallize into nanofibers because the final domain size is defined by the dimension of the nanofibrils with the fullerene domain acting like a space-filling glassy matrix. However, in cases where the polymer has a relatively low crystallinity or does not form nanofibers, it is also desirable to have the ability to systematically modify the crystallization of the fullerene phase.[31]

In this work we introduce C_{60} into the fullerene phase of P3HT/PCBM solar cells in order to systematically modify the crystal habit of PCBM. The solubility of C_{60} in chlorobenzene is only 6–7 mg/mL and this has limited its use in OSCs. Nevertheless, its use has been demonstrated as a pure n-type material for the fabrication of polymer solar cells via optimization of solvent conditions.[32] Because C_{60} is a precursor to PCBM and many other fullerene derivatives, it also has a lower associated cost and no additional synthesis requirements. We show using optical microscopy and UV-visible absorption spectroscopy that this approach alters the crystal morphology and greatly reduces the size of fullerene crystallites observed after very long annealing times and under aggressive aging conditions. We also show by fabricating organic field-effect transistors (OFETs) from PCBM/C_{60} blends that the incorporation of C_{60} does not significantly reduce electron mobility in bulk fullerene films. Finally, we show that when C_{60} is incorporated into the fullerene phase of P3HT/PCBM OSCs, devices are more stable to thermal degradation under annealing temperatures and aggressive aging conditions.

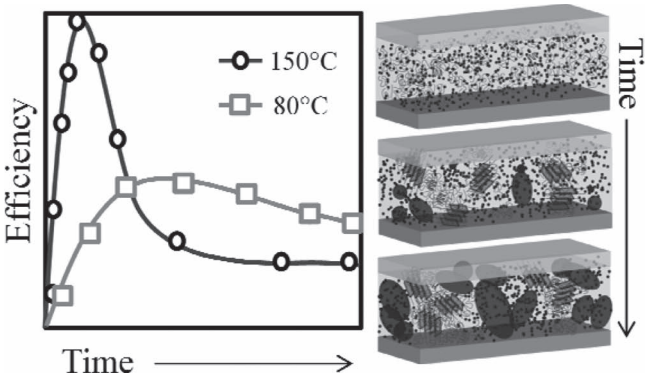

Figure 1. Schematic of phase segregation and coarsening occurring inside active layers (right) and for the changes in device performance that are expected to occur as a function of time at different temperatures (left).

2. Results and Discussion

2.1. P3HT/PCBM/C_{60} Film Characterization

Optical microscopy images and UV-visible absorption spectra (**Figure 2**) of P3HT/PCBM blends spin-coated on glass and annealed at 150 °C are shown in Figure 2A and Figure 2B respectively. We used these two techniques to monitor the extent of large-scale crystal overgrowth in the films. Image analysis applied to the microscopy images provided a means to quantify the total area occupied by visible crystallites, their number, and their average size, which is equivalent to the side length of a square with the same area as each crystallite. Specific signatures of PCBM overgrowth can also be observed in the UV-visible absorption spectra in Figure 2B. After the spectra are normalized to account for differences in film thickness, there is a clear decrease in absorbance at a wavelength of 336 nm. This peak is the lowest energy absorption feature for

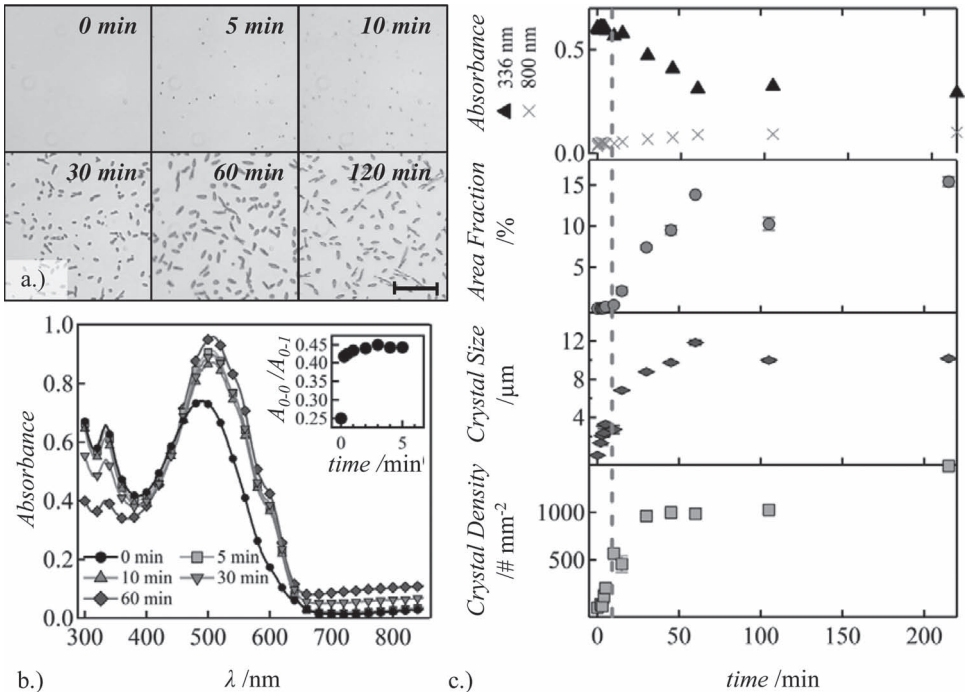

Figure 2. A) Optical microscopy images of P3HT/PCBM blends annealed at 150 °C at different times. Scale bar is 100 μm. B) UV-visible absorption spectroscopy of the films after annealing for different times–inset is the P3HT $A_{0\text{-}0}/A_{0\text{-}1}$ ratio vs. time (min). C) Summary of UV-visible absorption and optical microscopy data showing crystallite density, crystallite size, fractional area occupied by the crystallites on the film's surface, and the value of absorbance at $\lambda = 336$ nm. The dashed red line signifies the formation of visible PCBM aggregates on the film's surface.

PCBM and its decrease indicates migration of isolated PCBM molecules to join large PCBM crystallites. As seen in Figure 2C, the decrease in the peak at 336 nm that begins around 5 min (marked by the dotted red line) corresponds almost exactly with a slight increase in the absorbance background at higher wavelengths (<650 nm). This is expected as large PCBM aggregates will block or scatter a larger fraction of the incident light at all wavelengths.

Figure 2 shows that growth of micrometer-sized crystallites began after only 5 min of annealing. At this point, the P3HT achieved its maximum crystallinity as indicated by the $A_{0\text{-}0}/A_{0\text{-}1}$ ratio (inset, Figure 2B where $A_{0\text{-}0}$ = 605 nm and $A_{0\text{-}0}$ = 538 nm).[33] At this point, the number density and average size of visible crystallites increased rapidly. This also corresponded to a decrease in the PCBM absorption peak at 336 nm. After one hour of annealing, the PCBM absorption peak at 336 nm stopped decreasing, and a large number of 12 μm crystallites occupied 15% of the visible film area. The appearance of new micrometer-sized crystallites slowed at longer annealing times. This is likely a result of the depletion of all of the free PCBM within the film. Because optical microscopy is only sensitive to crystals larger than ~1 μm, this analysis does not account for nano-scale PCBM aggregates that are known to form during the early periods of annealing and could still be present even after long periods of annealing.[34] Therefore, these techniques can only quantify a limited region of the kinetics of growth of PCBM crystallites. Grazing incidence small angle X-Ray scattering (GISAXS) measurements were also performed on films to characterize morphological changes occurring at smaller length scales. Typical profiles for bulk heterojunctions containing pure PCBM and mixtures with C_{60} are included in the Supporting Information (Figures S.1 and S.2). These results support the existence of a morphological instability occurring in P3HT/PCBM films upon annealing and long term aging. Unfortunately, the exact mechanism of PCBM crystal growth is still a subject of debate and not fully understood. Nevertheless, microscopy and GISAXS data clearly demonstrate the importance of this crystallization process and provide valuable insight regarding the growth of large crystallites in bulk heterojunctions composed of P3HT/PCBM.

Figure 2 also shows that, after an initial nucleation period, visible PCBM crystallites grow larger and become more abundant. This growth must occur through the migration of dissolved PCBM from disordered regions of the polymer matrix until the chemical potential of PCBM in the amorphous P3HT is balanced with the chemical potential of PCBM in the crystalline phase. Therefore, the ultimate size and number of micrometer-sized crystallites observed in these films is a complex function of the solubility and mobility of PCBM in the polymer matrix, the number of nucleation sites, the crystallinity of the polymer within the film, and the film composition. Therefore, for the addition of C_{60} to the fullerene phase of polymer/fullerene blends to be effective, it must modify the growth kinetics of the fullerene crystallites such that the extent of fullerene overgrowth is reduced.

In order to quantify the extent of overgrowth that occurs when C_{60} is incorporated into the fullerene phase of P3HT/PCBM blends, we also fabricated P3HT/PCBM/C_{60} blends while maintaining a constant P3HT:fullerene weight ratio but varying

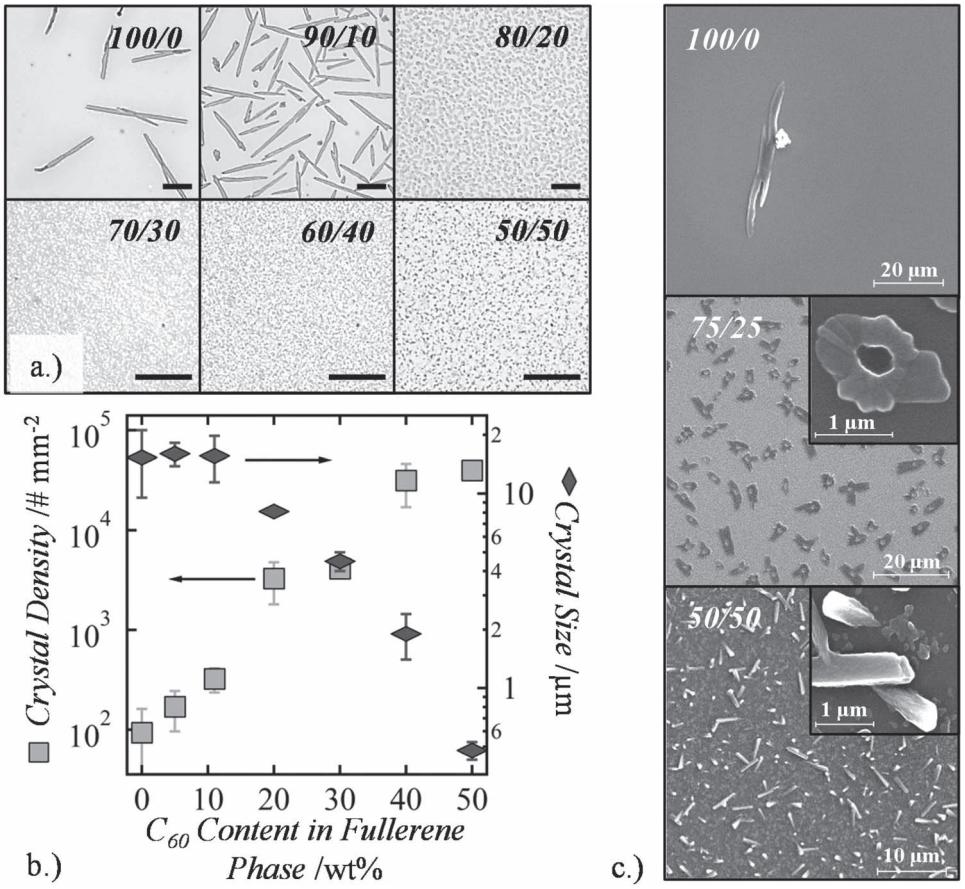

Figure 3. A) Optical microscopy images of films with varying PCBM/C_{60} content in the fullerene phase of a P3HT:fullerene film annealed for 2 h at 150 °C. Scale bar is 50 µm. B) Summary of the average crystal size and number of visible "overgrown" crystals at 2 h annealing. C) Scanning electron microscopy images of PCBM/C_{60} films after 1 h annealing at 150 °C on silicon wafers.

the PCBM/C_{60} content in the fullerene phase. **Figure 3**A shows the optical microscopy images of P3HT:fullerene films with increasing C_{60} content in the fullerene phase. These films were annealed at 150 ºC for 2 h. After applying the same analysis to these images as with pure P3HT/PCBM blends, Figure 3B shows the number density and the average size of visible micrometer-sized crystals as a function of PCBM/C_{60} content in the fullerene phase. Scanning electron microscopy images of PCBM/Fullerene films annealed at 150 °C for 1 h are also shown in Figure 3C to access smaller length scales. The extent of overgrowth is strongly dependent on the C_{60} composition in these films. From the optical microscopy images, it is clear that the presence of C_{60} causes a significant increase in the number density of crystallites while also simultaneously decreasing the average size of the visible overgrown crystals. The SEM images in Figure 3C also show that the morphology of the individual crystallites was significantly affected by the incorporation of C_{60} in the fullerene phase. As the C_{60} content is increased to 25 wt% in the fullerene phase, the crystallites are clearly much less needle-like and instead form disc-like or flower-like structures. As the C_{60} content in the fullerene phase increases to 50 wt%, the apparent crystal size decreases and the morphology becomes increasingly faceted. The degree to which crystals overgrow also appears to decrease but they tend to form faster during annealing (Figure S.3 in the Supporting Information). While the 100% PCBM films took more than 1 h at 150 °C to reach a fully stabilized morphology, very small quantities of C_{60} in the fullerene phase resulted in extensive crystallization within 5–10 min of annealing at 150 °C. However, once this initial growth ceased, the crystals maintained their smaller size even after very long annealing periods at 150 °C.

In order to test the stability of polymer/fullerene blends that incorporate C_{60} against accelerated aging conditions, P3HT:fullerene films with varying PCBM/C_{60} content were annealed at 150 °C and then aged at 90 °C. This temperature is somewhat higher than what is expected for typical solar-cell operating conditions but it is also lower than typical annealing temperatures. This experiment was also designed to test whether high-temperature annealing alone provided enhanced thermal stability for devices during operation since it had been previously proposed that annealing at higher temperatures stabilized P3HT/PCBM blends.[11] These films were again monitored using optical microscopy as shown in **Figure 4**. In order to better resolve small crystallites, SEM images were also taken for samples corresponding to the optical microscopy images of films annealed for 5 min at 150 °C and then aged at 90 °C. UV-visible absorption spectra were also obtained for these films and are presented in **Figure 5** along with the analysis of

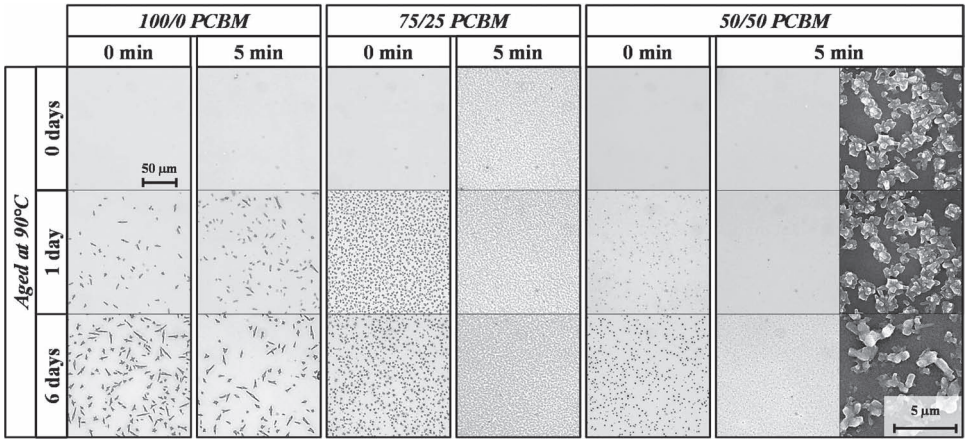

Figure 4. Optical microscopy images of films with varying PCBM/C_{60} that have been annealed at 150 °C and aged at 90 °C. Right column are scanning electron microscopy images of the 50/50 films annealed for 5 min and aged for varying times.

crystal size for each film. After 6 days of aging at 90 °C, the P3HT:fullerene films with 100/0 PCBM/C_{60} composition in the fullerene phase resulted in the same final aggregate size of ≈10 μm regardless of the annealing condition. This observation is contrary to some reports claiming that high temperature annealing stabilizes P3HT/PCBM blends to crystal overgrowth.[11] Interestingly, annealing the 50/50 PCBM/C_{60} blend did make the films significantly more stable to overgrowth when compared to films that were not annealed before aging. Aging the P3HT:fullerene blends with 50/50 PCBM/C_{60} ratio for 6 days resulted in crystals with an average size of 3 μm if they were not annealed first. However, identical films subjected to just 5 min of annealing at 150 °C resulted in ≈300 nm crystals after 6 days of aging. This represents an order of magnitude difference in crystal size with and without annealing.

The UV-Vis absorption spectra shown in Figure 5 provide further insight into the crystal overgrowth in Figure 4. Regardless of the composition of the fullerene phase, the absorption peak at 336 nm decreased and the average crystal size increased as a function of aging time when the films were not annealed. Therefore, aggregates large enough to be fully opaque to the spectrometer were forming throughout the films. For the annealed 100/0 PCBM/C_{60} film, the absorbance behavior was very similar to when it was not annealed. This is not surprising considering the long-time scale of PCBM overgrowth leaves plenty of free PCBM to continue to diffuse to growing crystallites when no C_{60} is present. For the annealed 75/25 PCBM/C_{60} film, after 5 min of annealing, large aggregates have already formed on the surface and the absorbance at 336 nm has already decreased. Therefore, aging the film at 90 °C had very little effect on the crystal size and absorbance at 336 nm. This was also the case for the 50/50 PCBM/C_{60} films. Interestingly, the absorbance at 336 nm stayed relatively constant even when compared when the film was not annealed. This verifies that the crystallites formed in this film are sufficiently small so that they are still transparent to the spectrometer and they are also more stable to further growth than films that do not incorporate C_{60}. The intermediate compositions shown in Figure 3b were also evaluated using this methodology and found to be consistent with the general trend that smaller, more numerous aggregates exhibit improved thermal stability.

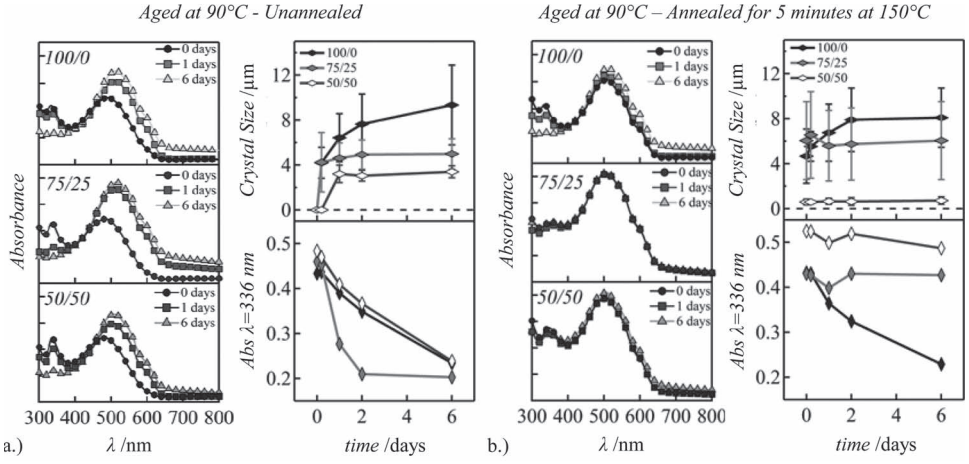

Figure 5. A) P3HT:fullerene films with varying PCBM/C_{60} content aged at 90 °C without annealing. B) P3HT:fullerene films with varying PCBM/C_{60} content annealed for 5 min at 150 °C and then subsequently aged at 90 °C.

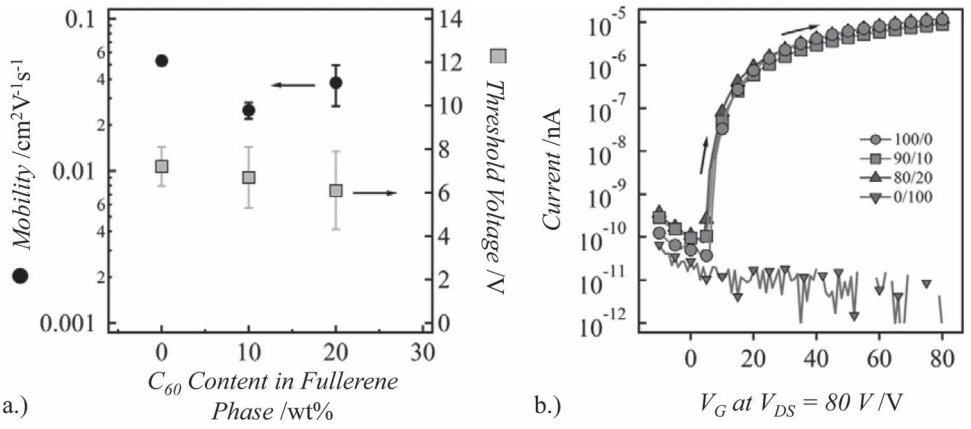

Figure 6. A) Electron mobility and threshold voltage as a function of PCBM composition. B) Forward sweep of transfer curve for OFETS made from PCBM/C_{60} blends of different composition.

2.2. PCBM/C_{60} Organic Field-Effect Transistors (OFETs)

To this point, this work has focused primarily on the characterization of the extent of overgrowth of PCBM crystallites from P3HT:fullerene films after different thermal treatments with varying PCBM/C_{60} composition in the fullerene phase. This characterization showed that, at relatively high C_{60} loadings, PCBM crystal overgrowth is reduced and the morphology is modified. Results also suggest that this approach could lead to more thermally stable OPVs. However, for this approach to be viable, the modification of the morphology of the fullerene phase must occur without a significant reduction of the electron transport properties in the fullerene phase. To test the effect of addition of C_{60} on the electron mobility of the PCBM phase, we fabricated organic field-effect transistors (OFETs) from PCBM/C_{60} solutions with varying C_{60} content (no P3HT). **Figure 6**A shows the measured field-effect mobility and threshold voltage from these devices and Figure 6B, the current–voltage (I–V) characteristic of representative devices. Overall, the electron mobility decreases slightly with the addition of C_{60} to PCBM with values of 0.05 cm^2/V s in pure PCBM and 0.03–0.04 cm^2/V s in the PCBM/C_{60} mixtures. This observation is not surprising given that prior theoretical work has also shown little effect of different polycrystalline structures on the electron mobility of pure C_{60} transistors.[35] The poor performance of the 0/100 C_{60} devices is a result of poor film adhesion to the substrate. In fact, films prepared with PCBM content below ≈75 wt% did not form films of sufficient quality to be tested using this approach. These measurements reveal small variations in the electron mobility values of a pure PCBM/C_{60} phase. However, it must be noted that, within a P3HT/fullerene bulk heterojunction, the electron mobility is also a complex function of the interconnectivity that exists between different fullerene domains, their orientation, size and shape. This is also equally true for the hole mobility corresponding to P3HT domains within bulk heterojunction devices. Generally, mobility measurements on P3HT/PCBM blends result in one order of magnitude reductions in the electron and hole mobility values with respect to measurements in the pure materials.[36] Therefore, the OFET measurements that we present here are only meant to characterize potential reductions in mobility that could occur within pure fullerene domains but these values are not really representative of the effective mobility that is measured in a bulk heterojunction device. The charge carrier mobility values in solar cells are affected by many other parameters and this makes it very difficult to isolate and characterize each contribution independently.

2.3. P3HT/PCBM/C_{60} Organic Solar Cells (OSCs)

The morphological studies of the effects of addition of C_{60} into the fullerene phase of P3HT/PCBM solar cells have, to this point, been based on experiments conducted on 'free' films coated on glass. There are a number of studies that show that the presence of a top electrode on P3HT/PCBM active layers can significantly affect the kinetics of PCBM diffusion and also modify the extent of vertical phase segregation.[37,38] It is therefore, difficult to directly infer device performance from only the observations of morphology in P3HT/PCBM active layers annealed without a confining top electrode. In order to test whether the incorporation of C_{60} into the fullerene phase of P3HT:fullerene films leads to more thermally stable OSCs, we have fabricated devices with an aluminum electrode evaporated onto the active layer before applying the thermal treatment (post-annealing). The performance of the OSCs was then tested after different thermal treatments. The first treatment consisted of an annealing time study at 150 °C. As shown in **Figure 7**A, the 100/0 PCBM/C_{60} devices show the best peak power conversion efficiency, 3.3% ± 0.3%, after 10 min of annealing. The 75/25 PCBM/C_{60} and 50/50 PCBM/C_{60} devices' peak efficiencies occurred after only 5 min of annealing and had values of 2.5% ± 0.4% and 2.2% ± 0.3% respectively. However, the performance achieved for the 50/50 PCBM/C_{60} devices after annealing for 120 min was still 91% of its original value whereas the performance of the 100/0 PCBM/C_{60} devices were already at 68% of their peak performance. We also performed an aging study where devices annealed for 5 min at 150 °C were subsequently placed at an elevated temperature (90 °C) for a longer time and tested periodically to evaluate

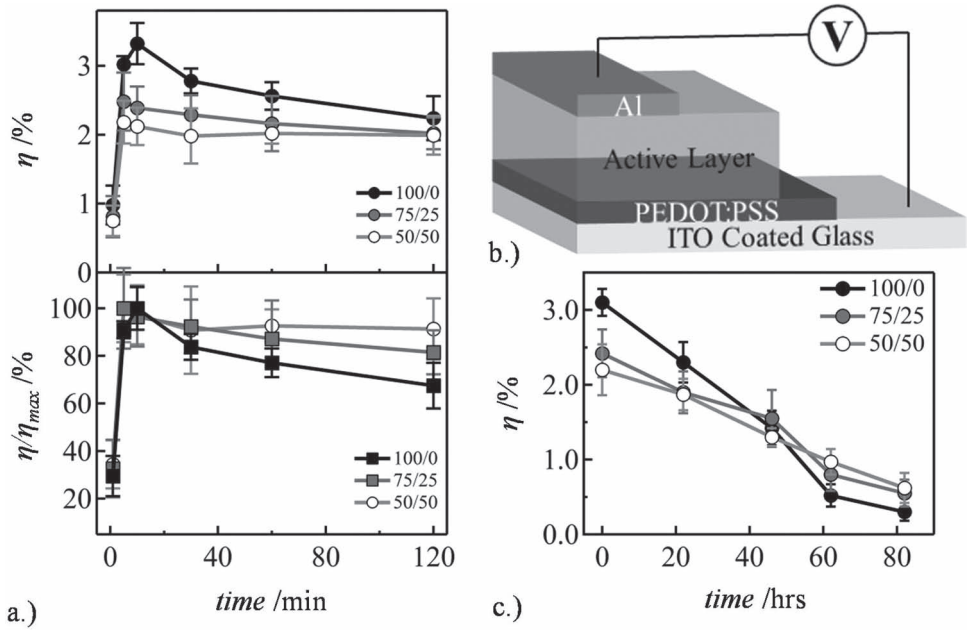

Figure 7. A) Efficiency and normalized efficiency of P3HT:fullerene devices with varying C_{60} content as a function of annealing time. B) Schematic of layers of OSCs fabricated for this study. C) Efficiency of P3HT:fullerene devices with varying C_{60} content as a function of aging time after being annealed for 5 min at 150 °C.

performance. The results of this test are shown in Figure 7D. After 80 h of aging, significant degradation of performance of all devices in the study was observed. The 100/0 PCBM/C_{60} devices' performance degraded 90% from 3.2% ± 0.2% to 0.3% ± 0.2%. Comparing these results to the devices incorporating C_{60}, the 72/25 PCBM/C_{60} devices degraded 78% from 2.4% ± 0.4% to 0.6% ± 0.2%, and the 50/50 PCBM/C_{60} devices degraded 71% from 2.2% ± 0.3% to 0.7% ± 0.2%. Therefore, under accelerated aging conditions, the 50/50 PCBM/C_{60} devices showed significant improvement over the 100/0 PCBM/C_{60} devices both in terms of relative performance to its peak efficiency and also in final efficiency.

The performance data shown in Figure 7 reveal that C_{60} incorporation into the fullerene phase of P3HT/PCBM solar cells can be used to improve the thermal stability of devices under accelerated aging conditions. The performance characteristics of P3HT/PCBM/C_{60} devices are also consistent with the observations made of open-faced films that were annealed and aged under similar thermal conditions. Particularly relevant is the absorbance of the PCBM peak at 336 nm. The 50/50 PCBM/C_{60} blend maintained a relatively constant absorbance that was greater than 100/0 PCBM/C_{60} films after extended periods of annealing and aging. In both cases, the maintenance of this peak is correlated to improved relative performance and in the case of aging, an overall better absolute efficiency. This suggests that the smaller crystal size formed in the 50/50 PCBM/C_{60} films observed with microscopy is also maintained in devices with confining electrodes that were made with the same composition. The improvement relative to the 100/0 PCBM/C_{60} films therefore likely results from an increased interface between P3HT/PCBM and possibly a prevention of mechanical damage to the devices as a result of very large aggregate growth. It is important to note that the devices fabricated here were prepared using the same optimized conditions for P3HT/PCBM solar cells without C_{60} incorporation. Therefore, the efficiency of devices incorporating PCBM/C_{60} devices could still be optimized to further improve the peak efficiencies achieved in these studies. Furthermore, it may be possible to also utilize other fullerene mixtures (C_{60}, C_{70}, $PC_{61}BM$, $PC_{71}BM$ and others) to further reduce the driving force to form crystals without affecting the electron mobility of the fullerene phase. This is the subject of ongoing research. In this work we highlight the modification of the P3HT/PCBM active layer by addition of C_{60} using the processing conditions that have been optimized for traditional devices.

3. Conclusions

In this work, we characterize the effects of C_{60} incorporation into the fullerene phase of P3HT/PCBM active layers as a simple approach to modify the growth of micrometer-sized PCBM crystallites. We find that incorporation of even small amounts of C_{60} had a dramatic effect on the nucleation and growth of PCBM crystallites. Increasing amounts of C_{60} in the bulk heterojunction films was also found to systematically modify the fullerene crystal size and morphology. We also showed that the P3HT:fullerene active layers that incorporated 50/50 PCBM/C_{60} in the fullerene phase had a greater thermal stability under aggressive aging conditions if they were annealed for a short time at 150 °C. We also fabricated OSCs that incorporate different amounts of C_{60} in their active layers and found that, under aggressive aging conditions, C_{60} offered improvements on the stability of devices when compared to devices fabricated without C_{60} incorporation. From open-film studies of P3HT/PCBM/C_{60} blends it appeared that the improved stability was

a result of a faster nucleation process that resulted in a larger number of much smaller fullerene crystallites. The size of fullerene crystallites ranged from 200 nm to 10 μm depending on the C_{60} loading and the crystallization conditions. Based on this work, we demonstrated that using mixtures of fullerenes in OSCs is a simple approach to improving the thermal stability of organic solar cells.

4. Experimental Section

Materials: Poly(3-hexylthiophene) (Sepiloid P100) used in this study was purchased from Rieke Metals (Lincoln, NE). [6,6]-Phenyl C_{61} butyric acid methyl ester was purchased from SES Research (Houston, TX) for the open films studies and American Dye Source for OSCs (Quebec, Canada). PEDOT:PSS (PVP AL 4083) was supplied by Clevios (Germany). The ITO used for solar cells was supplied by Colorado Concept Coatings (15 Ω m^{-2}) and was cut into 1.5 cm × 1.5 cm squares. Chlorobenzene, anhydrous, 99.8% was supplied by Sigma Aldrich (St. Louis, MO).

Fabrication and Characterization of Films: Two active layer solutions were prepared with identical P3HT:fullerene weight ratios. The first consisted of P3HT (18 mg) and PCBM (12 mg) in chlorobenzene (1 mL). The second consisted of P3HT (18 mg), PCBM (6 mg), and C_{60} (6 mg) in chlorobenzene (1 mL). Intermediate compositions were prepared by mixing different ratios of these two stock solutions. Therefore all films possess the same P3HT content, but varying PCBM/C_{60} content. These differences are reflected by labeling the relative weight fraction of the fullerene phase comprised of PCBM (e.g., 75/25 PCBM/C_{60} refers to 75 wt% PCBM and 25 wt% C_{60} in the fullerene phase). Films were spun-cast onto clean and dried glass slides at 1100 rpm for 60 s. Thermal treatments were applied in vacuo (<1 torr). Absorption spectroscopy measurements were made over a wavelength range of 300 nm to 1000 nm using a Thermo Scientific Evolution 300 UV-Vis spectrophotometer. Scanning electron microscopy (SEM) was performed using an FEI Sirion SEM. Optical microscopy images were obtained with using a Zeiss Axiovert 40 CFL Inverted Microscope.

Fabrication and Characterization of Organic Field-Effect Transistors (OFETs): Coating solutions were prepared by adding a mixture (10 mg total fullerene mass) of PCBM and C_{60} in chlorobenzene (1 mL) with different PCBM/C_{60} ratios except for a 0/100 PCBM/C_{60} solution which had a concentration of C_{60} (5 mg) in chlorobenzene (1 mL). Heavily n-doped silicon wafer was used as a substrate as well as a gate electrode. Thermally grown SiO_2 (200 nm) on the wafer acted as a gate dielectric layer. Surface of the oxide was cleaned by plasma for 4 min, coated with dilute benzocyclobutene (BCB; 1:20 vol/vol in mesitylene) by spin-coating (3 krpm for 60 s) in air, and thermally cured at 250 °C on a hotplate for 2 h under argon environment. PCBM/C_{60} solution was then spun onto the substrate (2 krpm for 60 s). OFETs were finished by depositing 35 nm thick gold electrodes through a shadow mask defining a transistor channel with a width of 1000 μm and a length of 100 μm. Electrical characteristics of OFETs were measured by using an HP4145B semiconductor parameter analyzer under nitrogen conditions.

Fabrication and Characterization of Polymer Solar Cells (PSCs): ITO coated glass substrates were cleaned via a series of ultrasonic baths in a mild detergent, deionized water, acetone, and isopropyl alcohol. The substrates were removed from the last bath and dried using N_2. They were then treated with air plasma for 10 min under vacuum (200 mTorr). Once clean, substrates were coated with filtered PEDOT:PSS. The PEDOT:PSS was spin-coated, in air, on top of the ITO surface from solution to obtain a layer roughly 40 nm thick. All solar cells maintained the same P3HT:fullerene weight ratio as was used for the open film microscopy studies. C_{60} content was varied on a wt% basis and the ratios refer to the PCBM/C_{60} ratio in the fullerene phase. Active layer solutions were stirred at 60 °C overnight in an inert atmosphere and filtered before use through a 250 nm PTFE syringe filter. These solutions were spin-coated at 1000 rpm for 60 s onto the PEDOT:PSS layer. 100 nm of aluminum was deposited via thermal evaporation under high vacuum (≈2×10^{-6} torr). The devices were then annealed at 150 °C for varying times under nitrogen. Aging at 90 °C was also carried out under nitrogen. The completed devices were immediately tested in air upon their completion using 100 W m^{-2} calibrated AM 1.5 light source.

Supporting Information

Supporting Information is available from the Wiley Online library or from the author.

Acknowledgements

The authors principally acknowledge funding from the Department of Energy Office of Basic Energy Sciences for financial support of this work under grant No. DE-SC0005153. This work was also funded under National Science Foundation (DMR-0120967 and SOLAR Award DMR 1035196). J.J.R. also acknowledges the National Science Foundation's Integrative Graduate Education and Research Traineeship for fellowship funding. The authors also acknowledge the Nanotech User Facility at the University of Washington, part of the National Nanotechnology Infrastructure Network for providing the STEM facilities.

Received: April 19, 2012
Revised: July 12, 2012
Published online: August 31, 2012

[1] F. Roberts, *J. Cryst. Growth* **1988**, *90*, 1.
[2] J. M. Wiencek, *Annu. Rev. Biomed. Eng.* **1999**, *1*, 505.
[3] Y. Wu, H. Yan, M. Huang, B. Messer, J. H. Song, P. Yang, *Chem. Eur. J.* **2002**, *8*, 1260.
[4] J. D. Bryan, D. R. Gamelin, *Prog. Inorg. Chem.* **2005**, *54*, 47.
[5] C. Brabec, N. Sariciftci, J. Hummelen, *Adv. Funct. Mater.* **2001**, *11*, 15.
[6] H. Hoppe, N. S. Sariciftci, *J. Mater. Res.* **2004**, *19*, 1924.
[7] A. J. Moule, K. Meerholz, *Adv. Mater.* **2008**, *20*, 240.
[8] A. Swinnen, I. Haeldermans, P. Vanlaeke, J. D'Haen, J. Poortmans, M. D'Olieslaeger, J. V. Manca, *Eur. Phys. J. Appl. Phys. 3* **2006**, *36*, 251.
[9] S. S. van Bavel, E. Sourty, G. de With, J. Loos, *Nano Lett.* **2009**, *9*, 507.
[10] U. Zhokhavets, T. Erb, H. Hoppe, G. Gobsch, N. S. Sariciftci, *Thin Solid Films* **2006**, *496*, 679.
[11] W. L. Ma, C. Y. Yang, X. Gong, K. Lee, A. J. Heeger, *Adv. Funct. Mater.* **2005**, *15*, 1617.
[12] T. A. Bull, L. S. C. Pingree, S. A. Jenekhe, D. S. Ginger, C. K. Luscombe, *ACS Nano* **2009**, *3*, 627.
[13] J. A. Lim, F. Liu, S. Ferdous, M. Muthukumar, A. L. Briseno, *Mater. Today* **2010**, *13*, 14.
[14] G. M. Newbloom, F. S. Kim, S. A. Jenekhe, D. C. Pozzo, *Macromolecules* **2011**, *44*, 3801.
[15] H. Xin, F. S. Kim, S. A. Jenekhe, *J. Am. Chem. Soc.* **2008**, *130*, 5424.
[16] H. Xin, O. G. Reid, G. Ren, F. S. Kim, D. S. Ginger, S. A. Jenekhe, *ACS Nano* **2010**, *4*, 1861.
[17] H. Xin, G. Ren, F. S. Kim, S. A. Jenekhe, *Chem. Mater.* **2008**, *20*, 6199.
[18] A. H. Rice, R. Giridharagopal, S. X. Zheng, F. S. Ohuchi, D. S. Ginger, C. K. Luscombe, *ACS Nano* **2011**, *5*, 3132.
[19] D. Chirvase, J. Parisi, J. C. Hummelen, V. Dyakonov, *Nanotechnology* **2004**, *15*, 1317.
[20] C. Muller, T. A. M. Ferenczi, M. Campoy-Quiles, J. M. Frost, D. D. C. Bradley, P. Smith, N. Stingelin-Stutzmann, J. Nelson, *Adv. Mater.* **2008**, *20*, 3510.

[21] J. Zhao, A. Swinnen, G. Van Assche, J. Manca, D. Vanderzande, B. Van Mele, *J. Phys. Chem. B* **2009**, *113*, 1587.
[22] D. Chen, F. Liu, C. Wang, A. Nakahara, T. P. Russell, *Nano Lett.* **2011**, *11*, 2071.
[23] N. Treat, M. Brady, G. Smith, M. Toney, E. Kramer, C. Hawker, M. Chabinyc, *Adv. Energy Mater.* **2011**, *1*, 82.
[24] E. Voroshazi, B. Verreet, T. Aernouts, P. Heremans, *Sol. Energy Mater. Sol. Cells* **2011**, *95*, 1303.
[25] S. Bertho, G. Janssen, T. J. Cleij, B. Conings, W. Moons, A. Gadisa, J. D'Haen, E. Goovaerts, L. Lutsen, J. Manca, D. Vanderzande, *Sol. Energy Mater. Sol. Cells* **2008**, *92*, 753.
[26] K. Sivula, Z. T. Ball, N. Watanabe, J. M. J. Fréchet, *Adv. Mater.* **2006**, *18*, 206.
[27] C. Yang, J. Lee, A. Heeger, F. Wudl, *J. Mater. Chem.* **2009**, *19*, 5416.
[28] J. H. Tsai, Y. C. Lai, T. Higashihara, C. J. Lin, M. Ueda, W. C. Chen, *Macromolecules* **2010**, *43*, 6085.
[29] C. Z. Li, S. C. Chien, H. L. Yip, C. C. Chueh, F. C. Chen, Y. Matsuo, E. Nakamura, A. K. Y. Jen, *Chem. Commun.* **2011**, *47*, 10082.
[30] Y. Zhang, H.-L. Yip, O. Acton, S. K. Hau, F. Huang, A. K. Y. Jen, *Chem. Mater.* **2009**, *21*, 2598.
[31] F. C. Jamieson, E. B. Domingo, T. McCarthy-Ward, M. Heeney, N. Stingelin, J. R. Durrant, *Chem. Sci.* **2012**, *3*, 485.
[32] L. G. Li, H. W. Tang, H. X. Wu, G. H. Lu, X. N. Yang, *Org. Electron.* **2009**, *10*, 1334.
[33] J. Clark, J. F. Chang, F. C. Spano, R. H. Friend, C. Silva, *Appl. Phys. Lett.* **2009**, *94*, 163306.
[34] W.-R. Wu, U. S. Jeng, C.-J. Su, K.-H. Wei, M.-S. Su, M.-Y. Chiu, C.-Y. Chen, W.-B. Su, C.-H. Su, A.-C. Su, *ACS Nano* **2011**, *5*, 6233.
[35] J. J. Kwiatkowski, J. M. Frost, J. Nelson, *Nano Lett.* **2009**, *9*, 1085.
[36] E. von Hauff, V. Dyakonov, J. Parisi, *Sol. Energy Mater. Sol. Cells* **2005**, *87*, 149.
[37] D. S. Germack, C. K. Chan, B. H. Hamadani, L. J. Richter, D. A. Fischer, D. J. Gundlach, D. M. DeLongchamp, *Appl. Phys. Lett.* **2009**, *94*, 3.
[38] M. Campoy-Quiles, T. Ferenczi, T. Agostinelli, P. G. Etchegoin, Y. Kim, T. D. Anthopoulos, P. N. Stavrinou, D. C. Bradley, J. Nelson, *Nat. Mater.* **2008**, *7*, 158.